Alanine Radicals: Structure Determination by EPR and ENDOR of Single Crystals X-Irradiated at 295 K

Einar Sagstuen,*,† Eli O. Hole,† Sølvi R. Haugedal,† and William H. Nelson‡

Department of Physics, University of Oslo, P.O. Box 1048 Blindern, N-0316 Oslo, Norway, and Department of Physics and Astronomy, Georgia State University, Atlanta, Georgia 30303

Received: July 2, 1997; In Final Form: October 10, 1997[⊗]

Single crystals of the amino acid L-α-alanine have been X-irradiated at room temperature, and the free radical formation has been studied using X-band and K-band EPR, ENDOR, and EIE (ENDOR-induced EPR) spectroscopy in the temperature interval 220−295 K. Aided by the results from EIE, as well as ENDOR from selected magnetic field positions, nine hyperfine coupling tensors were obtained and assigned to three different radicals. Room-temperature relaxation behaviors characterized by efficient W_{1x} and W_{1e} and by slow W_{1n} relaxation rates allowed for determination of the signs of the various hyperfine couplings from the ENDOR spectra obtained at room temperature. The temperature dependence of the W_{1x} relaxation is qualitatively discussed. The EPR spectra from alanine are dominated by the well-known resonance of the "stable alanine radical", SAR, formed by a net deamination of the protonated alanine anion. Precise hyperfine coupling tensors due to the α-proton coupling, the methyl group coupling, and a dipolar coupling to a methyl group of a neighboring molecule, as well as the *g* tensor, are given for this radical. Spectral simulations show that these parameters in a satisfactory manner reproduce all observable features of the resonance from this radical. Radical R2, apparently formed in roughly the same amounts as SAR, exhibits the structure $H_3N^+-{}^\bullet C(CH_3)C(=O)O^-$. It is formed from alanine by a net H-abstraction from the C_α position. The hyperfine coupling tensor to the freely rotating methyl group was obtained from both X-band and K-band data. K-band spectra obtained at several temperatures between 220 and 290 K revealed that the amino group is not freely rotating; that is, the three protons of the amino group are locked in their hydrogen bonds also after radical formation. A significant increase in ENDOR line widths upon increasing temperature made the ENDOR lines due to the amino protons practically nonobservable at 295 K. However, the three corresponding hyperfine coupling tensors were easily obtained from K-band ENDOR data at 220 K. The B_0 and B_2 values for β-coupling to N^+-H fragments were determined to be −4.3 and 117.6 MHz, respectively. Due to partly unresolved nitrogen hyperfine interaction leading to larger line widths, the individual EPR lines from radical R2 are of far less intensity as compared to those of the SAR. However, simulations strongly indicate that there is an almost equal relative distribution (60%:40%) of the two radicals. Two hyperfine coupling tensors were assigned to two conformations of a third minority radical species (radical R3) which tentatively is suggested to be the species $H_2N-{}^\bullet C(CH_3)C(OH)=O$. Possible mechanisms for the formation of the radicals are discussed in light of the basic radiation chemistry of the amino acids. The simultaneous presence of two stable radicals of similar relative amounts in alanine may have consequences for the use of alanine as a radiation dosimeter.

1. Introduction

The solid-state radiation chemistry of the simple amino acid L-α-alanine (see structure below) has been studied for many years using electron paramagnetic resonance (EPR) spectroscopy and related techniques.[1−13] In the later years, particular interest has been shown in this compound due to its radiation dosimetric properties.[14] Good dose−yield factors, linear signal response over a wide range of radiation doses, excellent fading characteristics, and small dependency of temperature, humidity, and light, radiation quality, and dose rate as well as a high level of dose saturation are all important properties for EPR dosimeters.[14,15]

For dosimetric purposes, the EPR powder spectra from amorphous alanine pellets or other types of alanine samples are used. In this powder (disordered solid) spectrum readout, the amplitude of the central line is usually used for monitoring the radiation dose. For illustration purposes, an example of a powder spectrum is shown in Figure 1d.

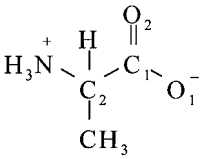

ℓ-α-Alanine

It has commonly been assumed that the polycrystalline EPR from alanine is due to one single radiation induced free radical, the so-called SAR, the stable alanine radical. This species has been shown to exhibit structure **1**, formed by deamination from a protonated alanine radical anion.[1−4,9,11,16]

The EPR of the SAR is mainly due to interactions of the unpaired electron with the proton bonded to C2 and with the three equally coupled (rotationally averaged) methyl protons.

Due to peculiarities in both the radiation dose dependency and the microwave power dependency of the powder-EPR from

* To whom all correspondence should be addressed.
† University of Oslo.
‡ Georgia State University.
⊗ Abstract published in *Advance ACS Abstracts,* December 1, 1997.

S1089-5639(97)02158-0 CCC: $14.00

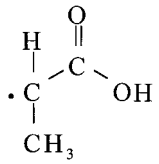

Structure 1

Stable Alanine Radical

alanine pellets, it has been speculated if several resonances possibly could be present simultaneously.[2,17−19] This was also suggested in the authorative work by Kuroda and Miyagawa.[11] Radiation chemistry studies in frozen solutions, glasses, and aqueous solutions of alanine have revealed that several radical species invariably are formed.[20,21] Solid-state radiation damage processes in amino acids have been studied for many years.[16,22] In most cases, the room-temperature radical population consists of several species originating from both the pristine reduction and the pristine oxidation products. The SAR is generally believed to originate from the reductive chain.[9,22,23] None of the previous solid-state radiation damage studies have, however, paid much attention to eventual minority radical species residing together with the SAR. Also, hyperfine coupling and *g* tensor data sufficiently precise for computer simulation of X- and Q-band room-temperature EPR spectra of the SAR are not available in the literature.[18]

In a previous paper[24] preliminary hyperfine coupling and *g* tensors for the SAR were presented and used to discuss the microwave saturation behavior of this radical. It was shown by simulations that at high microwave powers weakly allowed transitions (nuclear "spin flips"[25] as well as "second-order transitions"[1,2,26]) gained relatively high intensities, in part explaining some features of the high-power EPR from alanine. However, there are still features which cannot be assigned to forbidden transitions in alanine.

As experience suggested to us the high probability of the presence of several radical species in solid alanine at room temperature, it was decided to undertake a detailed EPR and ENDOR study of radical formation in single crystals of alanine at room temperature. For the first time, this study clearly shows that at least two radicals are present together with the SAR, and the data leading to their identification are presented. One of these new radicals, R2, is in fact present in relative amounts comparable to that of the SAR. This may have considerable importance with respect to the use of EPR/alanine dosimetry in applications with inherently high demands of accuracy, e.g. for therapeutic purposes.

2. Experimental Section

Single crystals of L-α-alanine were obtained by slow evaporation of aqueous solutions of the commercial compound (Sigma Chem. Co.). Partially deuterated crystals were obtained by repeated (>3×) recrystallizations from 99.9% D_2O (Sigma Chem. Co.). Under the present crystal growth conditions, no D-exchange of the central H atom (HC2) is expected. The crystal structure has been solved using X-ray diffraction by Simpson and Marsh[27] and Dunitz and Ryan[28] and by neutron diffraction by Lehmann et al.[29] The crystallographic coordinates from the neutron diffraction study were used in the present work. The crystals are orthorhombic with space group $P2_12_12_1$. The unit cell axes were used as the orthogonal reference system in this study. In addition, a fourth rotation axes, skewed with respect to the reference system axis, was used to assign unique hyperfine coupling tensors and solve the so-called Schonland ambiguity.[30]

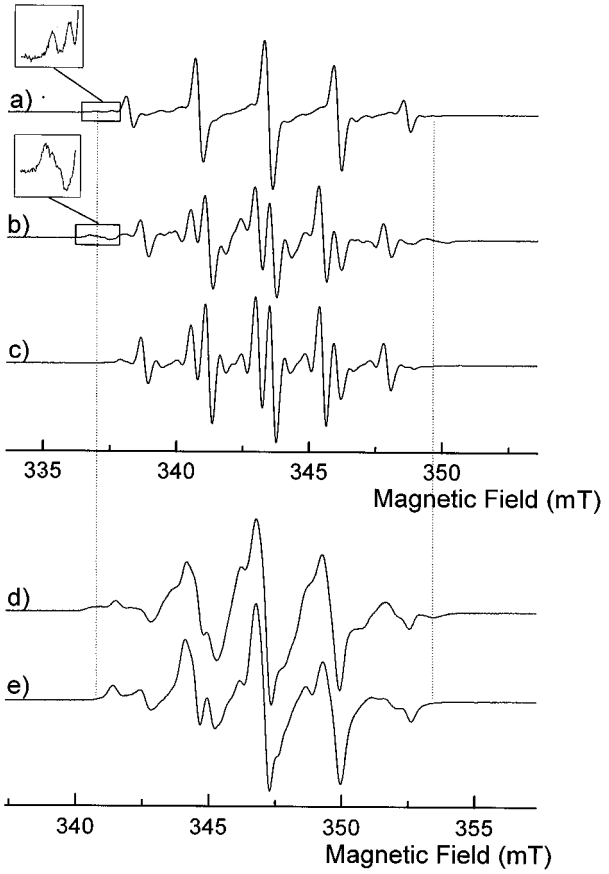

Figure 1. First-derivative X-band EPR spectra from L-α-alanine X-irradiated and measured at 295 K. Each spectrum sweep is centered at $g = 2.0023$. (a) Nondeuterated single crystal with the external field parallel with crystallographic ⟨*c*⟩ axis. (b) Nondeuterated crystal, external field parallel with ⟨*a*⟩. (c) Deuterated crystal, external field parallel with ⟨*a*⟩. (d) Polycrystalline, nondeuterated sample, dose = 6.3 kGy. (e) Polycrystalline deuterated sample.

TABLE 1: Coordinates (in Å) of the Stable Alanine Radical (SAR) as Obtained from the Data of Ref 11

atom	*x*	*y*	*z*
C1	2.93	1.44	4.05
O1	3.95	0.79	3.77
O2	2.79	2.04	5.15
C2	1.80	1.51	3.02
H	0.90	2.08	3.27
Cm[a]	1.97	0.76	1.69
Cm(II)[b]	1.36	−1.13	4.64

[a] This is the carbon atom of the methyl group. [b] This is the carbon of the methyl group of the symmetry equivalent molecule at position II, ((1/2)-x, -y, (1/2)+z).[11]

Kuroda and Miyagawa have performed a very detailed ENDOR analysis of the weak couplings associated with the stable alanine radical after X-irradiation at 295 K, measured at 77 K.[11] These authors deduced the coordinates of the stable alanine radical (SAR) in the unit cell and showed that considerable molecular reorganization as compared with the coordinates of the pristine molecule had taken place. For convenience, a summary of the most pertinent results of their calculations is reproduced in Table 1. As discussed below, some of these coordinates have been used for the comparison with hyperfine coupling data obtained in the present work.

The crystals were X-irradiated with 60 kVp, 40 mA X-rays from a Phillips tungsten X-ray tube to doses up to about 40 kGy (30 kGy/h). They were then mounted on X-diffraction goniometers, and aided by X-diffraction photographs, the rotation axes were aligned with each of the crystal axes to within

0.5°. In the X-band experiments, the crystals were then transferred to quartz crystal holders without loss of rotation axis alignment. These quartz rods were part of a one-axis goniometer allowing for rotation of the crystal about an axis in the EPR/ENDOR cavity, with a precision of rotation better than 0.5°. In the K-band experiments, the crystals were transferred to an OFHC copper post without loss of rotation axis alignment. This copper post was mounted to the Joule-Thompson tip of an Air Products helium refrigerator. Powder spectra were obtained using commercial alanine dosimeter pellets (Bruker GmbH, quality bronze) given X-ray doses between 1 and 10 kGy. To obtain powder spectra from deuterated samples, irradiated deuterated crystals crushed in a porcelain mortar were used.

X-band EPR, ENDOR, and ENDOR-induced EPR (EIE) measurements were performed using a modified Bruker ER 200 D-SRC spectrometer together with the Bruker EN-200 accessory, as previously described[31a] but now equipped with a 100 W ENI 3100L rf-generator. Regularly, EPR spectra were obtained using 100 kHz modulation frequency, with a modulation amplitude (p−p) in the range 0.07−0.125 mT using a microwave power of 26 dB (below 215 mW). ENDOR spectra were run using a microwave power of 5 dB, with frequency modulation at 12.5 kHz using 150 kHz modulation depth and with the rf-power being on the order of 60 W.

K-band EPR, ENDOR, and EIE measurements were performed using instrumentation and methods as previously described in detail.[31b] In addition, a Hughes 24 dB low-noise microwave preamplifier and a balanced mixer design of the detector have recently been implemented.

The *g*-tensor was obtained from the EPR spectra and the hyperfine coupling tensors from ENDOR spectra using the program MAGRES.[32] When available, both the low-frequency and the high-frequency ENDOR lines due to one hyperfine coupling were used for tensor calculations. The tensors obtained from the two branches agreed within one standard deviation. Only tensors obtained from the high-frequency ENDOR lines are given in Tables 2−4. The rms values for the fitting of all tensors to the ENDOR data were less than 50 kHz. Simulations of EPR spectra were performed using the program described previously.[24]

It should be noted that due to the nonlinearity of the rf-power amplifier used for the X-band ENDOR studies, second-harmonics of the strongest ENDOR lines were observed. These are marked with * in the X-band ENDOR spectra shown in the Figures.

3. Experimental Results and Analysis

The EPR spectra from crystalline alanine are well-known from previous publications.[1,2] Figures 1a,b shows spectra recorded (using a nondeuterated crystal) with the external magnetic field along two of the crystal axes, ⟨*c*⟩ and ⟨*a*⟩ . The dominating feature of the ⟨*c*⟩-axis spectrum (Figure 1a) is a quintet, due to four near-equivalent proton couplings, the α-proton, and the three protons of the freely rotating methyl group. In the ⟨*a*⟩-axis spectrum (Figure 1b) the quintet is split into a doublet of quartets since the α-proton coupling is far smaller than the methyl proton coupling at this orientation.

The spectra in Figure 1a,b show weaker resonance features in addition to those forming the basic quintet, or doublet of quartets, spectra. Several of these are due to "proton spin flips", characterized by satellites flanking a major EPR transition by $\pm g_N\beta_N B$, or about ±0.5 mT at X-band microwave frequencies.[25] These transitions, which thus also are associated with the SAR, are due to a nearly pure dipolar interaction with proton(s) in one or several neighboring molecules. Other features occurring between the main EPR transitions of SAR are due to so-called (and misnamed) "second-order" transitions, as discussed in detail by previous authors.[1,2,26] These points will be further commented on below. However, the spectra in Figure 1a,b also show distinct features outside of the resonance of the SAR. These have been highlighted with dotted lines and amplifying insets. Figure 1d shows a powder spectrum from an alanine pellet, and the corresponding extreme outer features are also clearly observed in this spectrum. Figure 1c shows the spectrum along ⟨*a*⟩ from a partially deuterated crystal. It is important to note that in this figure the extreme outer features are completely missing, indicating that these features in part are due to interaction with the easily exchangeable amino protons. Figure 1e shows the powder spectrum from a deuterated sample. Again, the outer features of Figure 1d are absent.

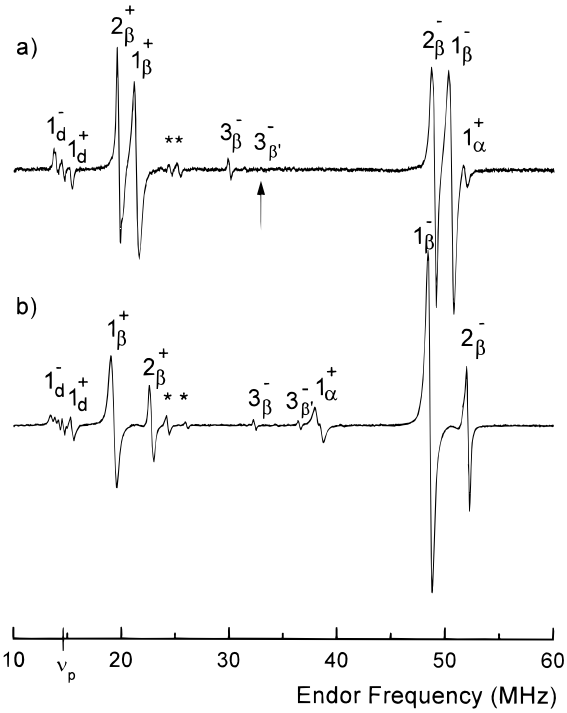

Figure 2. X-band ENDOR spectra from a nondeuterated single crystal of L-α-alanine, X-irradiated and measured at 295 K. The external magnetic field has been fixed to one of the central resonance lines of the EPR spectra in Figure 1a,b. Resonance lines have been marked as described in the text of section 3. Lines marked with * are due to second harmonics of the two strongest ENDOR lines in the region about 50 MHz. (a) External magnetic field parallel with ⟨*c*⟩, and (b) field parallel with ⟨*a*⟩.

Figure 2 shows X-band ENDOR spectra recorded at 295 K by locking the magnetic field to the central line of each of the EPR spectra in Figure 1a,b. Nine resonance lines assigned to six different hyperfine coupling tensors have been analyzed from the X-band data. In Figure 2, each of the resonance lines have been marked with a number, indicating to which radical it is assigned; a superscript + or −, indicating whether the line is assigned to the $M_s = +1/2$ or $-1/2$ energy level manifold, and a subscript indicating the type of coupling, (α) alpha, (*β*) beta, or (d) distant methylinteraction. The lines marked with * are second-harmonics of the two strong high-frequency ENDOR lines. In the following paragraphs, arguments for these assignments will be presented.

3.1. Radical R1: The Stable Alanine Radical, SAR. Three interactions have been assigned to radical R1 based on results from ENDOR data obtained by locking the field to various positions in the EPR spectrum (see paragraph 3.4 below) as

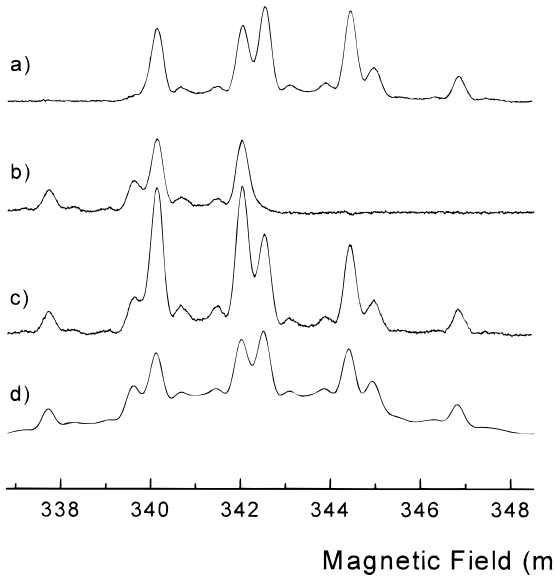

Figure 3. X-band ENDOR−induced EPR (EIE) spectra from a nondeuterated single crystal of L-α-alanine, X-irradiated and measured at 295 K, compared to a simulated EPR absorption spectrum. The external magnetic field is parallel with ⟨*a*⟩. (a) EIE obtained by monitoring the high-frequency ENDOR line due to radical R1 (line 1_β^- in Figure 2b). (b) EIE obtained by monitoring the low-frequency ENDOR line due to radical R1 (line 1_β^+ in Figure 2b). (c) Sum of the two EIE spectra in a and b. (d) Simulated EPR absorption pattern due to radical R1, obtained by using the tensor data in Table 2.

well as from EIE results. Figure 3a,b shows EIE spectra obtained from respectively the 1_β^+ and the 1_β^- ENDOR lines in Figure 2b. Similar spectra were obtained from the 1_α^+, 1_d^+, and 1_d^- lines. The very asymmetric features of these EIE spectra obtained at room temperature are due to the specific relaxation rates in this system. This will be considered in more detail in section 3.4. Here, it suffices to note that adding the two EIE spectra in Figure 3a,b, a relatively symmetrical spectrum (Figure 3c) is obtained which is representative for the complete EIE of radical R1. This was confirmed by K-band EPR/ENDOR and EIE measurements performed at 220 K, as described below. It is evident from the EIE spectrum in Figure 3c that the resonance of radical R1 is that of the dominating doublet of quartets in Figure 1b.

The hyperfine coupling tensors arrived at from the analysis of the ENDOR in the four planes of rotation are given in Table 2 together with the *g* tensor obtained by analyzing the EPR spectra. (Due to refinements of the data analysis, some of the tensors in Table 2 are slightly different from the preliminary results given in a previous publication.[24]) The data in Table 2 uniquely characterize the SAR through the excellent internal correlation of the principal axes, as well as the very good agreement with the coordinate data of Kuroda and Miyagawa[11] given in Table 1. The *g* tensor shows small anisotropy, characteristic of small organic radicals containing heteroatoms. The eigenvector for the minimum g value (g_{min}) is expected to be parallel to the lone electron orbital (LEO) for a π-type radical.[33] The H_α tensor is a typical α-proton coupling tensor of a planar π-radical.[26] From the isotropic value, the $2p^\pi$ spin density can be estimated to 0.78, using the McConnell relation with $Q = -72$ MHz.[34] Using the dipolar coupling tensor, the spin density is calculated to 0.72.[35] For a planar π-radical the eigenvector of the intermediate principal value for an α-proton coupling tensor and the eigenvector of g_{min} are both expected to be along the lone electron orbital, LEO.[26] For R1 these directions deviate less than 3°. Furthermore, the two directions are close to perpendicular to the C1−C2−Cm plane (about 12° deviation). The eigenvector of the minimum α-proton coupling principal value, expected to be along the C−H bond, is virtually identical with that which may be calculated for the C2−H bond direction from the data in Table 1.

TABLE 2: Magnetic Parameters for Radical R1, the Stable Alanine Radical (SAR), from EPR and ENDOR Measurements at 295 K[a,b]

	isotropic	principal	eigenvector[c]		
tensor	value	values	⟨*a*⟩	⟨*b*⟩	⟨*c*⟩
g	2.0033	2.0041	0.828	0.030	0.559
		2.0034	−0.428	0.678	0.598
		2.0024	0.362	0.735	−0.574
H_α	−56.1(3)	−87.9(2)	0.467(4)	0.416(6)	0.780(4)
		−52.2(4)	0.310(11)	0.749(8)	−0.586(6)
		−28.2(6)	0.828(5)	−0.515(11)	−0.221(8)
H_β	69.9(1)	74.7(2)	−0.173(20)	0.581(13)	0.795(09)
		67.6(2)	−0.896(230)	−0.428(400)	0.117(340)
		67.3(2)	0.408(500)	−0.693(240)	0.594(66)
H_{dip}	0.1(1)	5.0(2)	0.203(25)	0.810(15)	−0.551(20)
		−2.1(3)	0.921(180)	−0.348(260)	−0.172(446)
		−2.5(3)	0.331(500)	0.472(195)	0.817(93)

[a] Hyperfine coupling tensor elements are given in units of MHz. [b] Uncertainties are given at the 95% confidence level in the last digit(s) of the quoted values [c] Directions calculated from the atomic position coordinates in Table 1:

C2−Cm bond direction	−0.1107	0.4882	0.8657
C2−H bond direction	0.8225	−0.5209	−0.2285
C2···Cm(II) direction	0.1407	0.8439	−0.5178
perpendicular to plane of C1−C2−Cm	0.4192	0.8126	−0.4048

The H_β tensor is assigned to the coupling between the electron and the three equally coupled methyl protons of the freely rotating methyl group. The tensor is a typical β-proton coupling tensor, and as expected the direction of the maximum principal value is close to the C2···Cm direction[34] calculated from the data in Table 1 (about 8° deviation).

The third coupling is nearly purely dipolar in nature. This dipolar nature of the coupling is indicative of an intermolecular interaction. Using the coordinates of Kuroda and Miyagwa,[11] the direction of the maximum principal value of H_{dip} is very close (about 4° deviation) to the intermolecular direction between the central carbon atom C2 of the radical and the carbon of the methyl group of an undamaged neighboring alanine molecule (Cm(II), see Table 1). From the dipolar tensor, the effective interspin distance *r* can roughly be estimated from the relation[11,25]

$$a_d = 80\rho^\pi/r^3[\text{MHz}]$$

where a_d is the dipolar coupling and ρ^π is the $2p^\pi$ orbital spin density at the central carbon atom. Using the medium value 0.75 for the spin density and $a_d = 2.5$ MHz from Table 2, *r* becomes about 2.9 Å. This agrees well with the C2−Cm(II) distance of 3.13 Å, calculated from Table 1.

The available data leave no doubt about the interpretation of radical R1 as the SAR, shown in structure **1**. The "proton spin flip" resonance lines are well-known to arise from protons weakly coupled to the unpaired electron mainly by dipolar interactions.[25] The proton coupling described by the H_{dip} tensor in Table 2 is an excellent candidate for the origin of these features of the EPR spectra. This interpretation is corroborated by the observation that the satellites are present also in partially deuterated crystals. Similarly, it is well-known that the so-called "second-order" transitions observed between the main lines of the SAR are the less intense inner pair of the quartet of EPR transitions associated with an anisotropic proton interaction.[1,2,26]

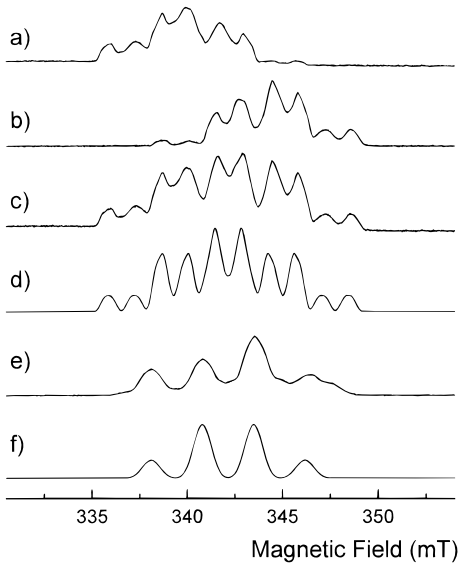

Figure 4. X-band ENDOR-induced EPR (EIE) spectra from single crystals of L-α-alanine, X-irradiated and measured at 295 K, compared to simulated EPR absorption spectra. The external magnetic field is parallel to ⟨*a*⟩. (a) EIE obtained by monitoring the low-frequency ENDOR line due to radical R2 (line 2_β^+ in Figure 2b). (b) EIE obtained by monitoring the high-frequency ENDOR line due to radical R2 (line 2_β^- in Figure 2b). (c) Sum of the two EIE spectra in a and b. (d) Simulated EPR absorption pattern due to radical R2, obtained by using the tensor data for radical R2 in Table 3, together with a nitrogen hyperfine interaction as described in the text. (e) Sum of the two EIE spectra obtained by monitoring the low-frequency (2_β^+) and high-frequency (2_β^-) ENDOR lines due to radical R2 using a partially deuterated crystal. (f) Simulated EPR absorption pattern due to a partially deuterated radical R2. The simulation used the tensor data for radical R2 in Table 3, but with the principal values for amino proton couplings replaced with values corresponding to deuterium hyperfine interactions.

Both types of these transitions are accounted for when the nuclear Zeeman term is included in the evaluation of the hyperfine splitting, even to first order. Using a simulation program including such effects, it was shown in a previous paper[24] that all EPR spectra of the SAR are excellently reproduced using the data in Table 2. The EIE spectrum in Figure 3c is directly comparable to the simulated absorption EPR spectrum of the SAR,[24] as shown in Figure 3d.

3.2. Radical R2: The H-Abstraction Radical. Figure 1 shows clear resonance features outside of the resonance from the SAR (in nondeuterated crystals) which are due to a second radical species. For $B\|\langle a\rangle$, these outer resonance features are about 12.5 mT apart, and thus extensive hyperfine interaction is necessary to allow for this spectral width. As the outer features remain weak in all EPR spectra, no structural analysis could be performed from the EPR spectra alone. However, since the total spectral span varies very little through all three planes of rotation, it is less probable that an α-proton interaction is present. Also, as demonstrated in Figure 1c,e, these outer features are completely missing in partially deuterated samples, indicating couplings to the easily exchangeable amino protons.

With X-band ENDOR at room temperature, locking the external magnetic field to each of the extreme outer features of the EPR spectrum, the ENDOR resonance lines denoted 2_β in Figure 2 were the only ones detected (see also Figure 8, traces 1 and 5). The analysis of these resonance lines yielded the first H_β hyperfine coupling tensor shown in Table 3. This coupling is assigned to a β-type coupling to the methyl group. It is very similar to the H_β coupling of radical R1 (Table 2), but the direction of the maximum coupling is closer to that of the C2−Cm bond direction in the native crystal (see below), indicating less reorganization upon formation.

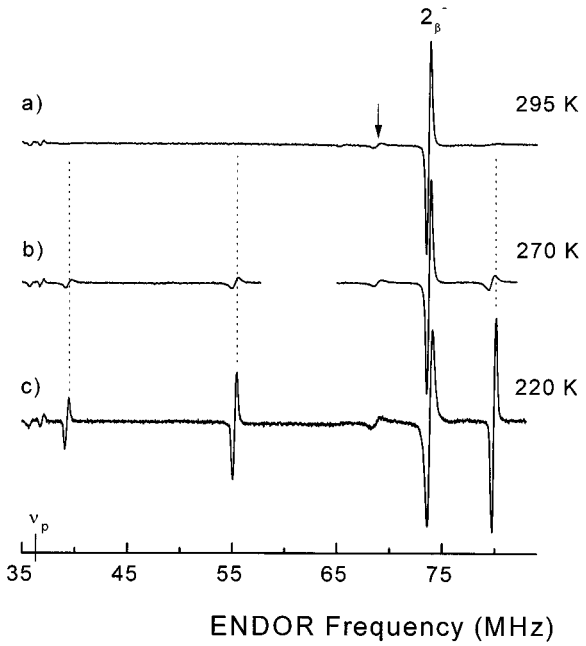

Figure 5. K-band ENDOR spectra of a single crystal of L-α-alanine, X-irradiated at 295 K and measured at the temperatures indicated. $B\|\langle a\rangle$. The magnetic field was locked to the high-field extreme feature of the EPR spectrum, due to radical R2. The arrow indicates a resonance line-like feature, which is an instrumental artifact.

It was very difficult to get EIE spectra from radical R2 at room temperature, due to the same peculiarities of the relaxation times as for radical R1 (see section 3.4). Figure 4,b shows X-band EIE spectra associated with R2 obtained at room temperature by locking the rf to respectively the 2_β^+ ENDOR line and the 2_β^- ENDOR line ($B\|\langle a\rangle$). The very asymmetric features of these EIE spectra are, as for radical R1 above, due to the specific relaxation rates in this system (see below). Adding the two EIE spectra in Figure 4a,b, the spectrum in Figure 4c is obtained, taken as representative for the complete EIE of radical R2 (see also the K-band spectra in Figure 6).

The 10-line EIE in Figure 4c indicates the presence of further hyperfine interaction for radical R2. As judged from the isotropic value of the H_β coupling tensor, the C2 spin density is nearly the same as that for radical R1, about 0.75. As the magnitude of the β-methyl coupling implies that about 15% of the spin density is located in the 1s orbitals of the three hydrogens, only a small fraction of the spin density is left to account for the additional 5 mT additional spectral width (maybe about 10%, taking into account some delocalization onto the carbonyl moiety). Having dismissed the possibility for an α-coupling, the only interaction possible to account for such a large spectral width is β-type couplings to the three protons of the amino group. The ENDOR spectra at 295 K, however, revealed no other resonance lines which might be ascribed to such interactions. To increase the intensity of any eventual ENDOR lines not observable at room temperature, a cooling experiment was performed. In a sequence of experiments using a K-band EPR/ENDOR spectrometer, cooling the crystal from 290 to 220 K (in 10 K steps), dramatic changes occurred in the ENDOR spectra, *even though the EPR remained unchanged*. These observations are illustrated in Figure 5. All ENDOR spectra were recorded off the high-field extreme feature of the EPR spectrum (in these experiments, the free proton frequency is 36.3 MHz). The K-band ENDOR spectrum obtained at 290

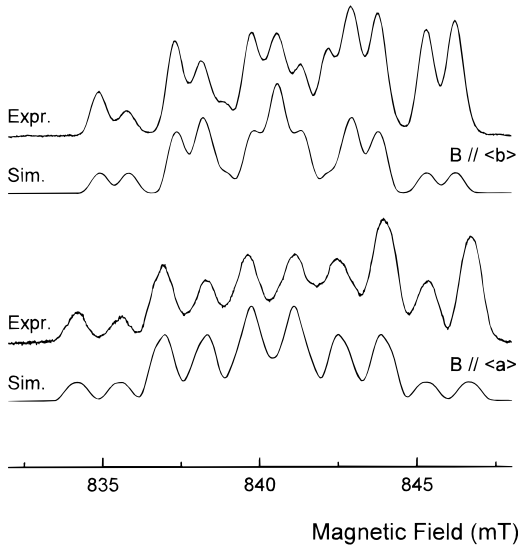

Figure 6. Experimental K-band EIE spectra and simulated K-band absorption EPR spectra from a nondeuterated single crystal of L-α-alanine X-irradiated at 295 K and measured at 220 K. The external magnetic field is directed along ⟨*b*⟩ (top) and ⟨*a*⟩ (bottom). The simulated spectra were calculated using the tensor data in Table 3, together with a nitrogen hyperfine interaction as described in the text.

K corresponds as expected closely to the X-band spectrum obtained at room temperature, shown at the bottom in Figure 8 (marked 5). However, three new ENDOR lines grew in upon cooling, and the intensity increased with decreasing temperature. Apparently, decreasing the temperature from 290 K decreases the line width of these specific ENDOR lines, rendering them observable only at temperatures below room temperature. Decreasing thermal libration may increase the nuclear relaxation time T_{1n} for these protons and thus decrease the ENDOR line width at temperatures below room temperature. In a cooling experiment in the temperature range 295−10 K it was observed that the freely rotating methyl started to become hindered at temperatures below 200 K. Thus, to obtain as intense ENDOR signals as possible from the three extra ENDOR lines, but at the same time make sure that the geometrical properties of the radicals were identical with those at room temperature, the hyperfine coupling tensors associated with the three ENDOR lines were evaluated at 220 K and are given in Table 3. For comparison with the X-band data obtained at room temperature, the H_β coupling to the methyl coupling was also obtained from the K-band spectra at 220 K (second tensor in Table 3), and as expected the X-band and K-band tensors are virtual identical. The other three hyperfine coupling tensors are all in agreement with β-proton couplings to the amino protons. Comparing the three eigenvectors for the maximum β-couplings with the three C2···H directions, the deviations are less than 9° for all three tensors when using the crystallographic C2···H directions and less than 12° for all when using the recalculated C2···H directions given in Table 3. K-band ENDOR experiments at 220 K using partially deuterated crystals showed that the three ENDOR lines were absent. Thus the three ENDOR lines must be due to couplings with the three amino protons, and the proposed structure of radical R2 must be structure **2** below:

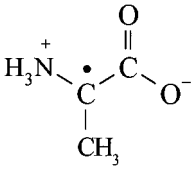

Structure 2

TABLE 3: Magnetic Parameters for the Radical R2 in X-Irradiated Single Crystals of L-α-Alanine from X-band and K-band ENDOR Measurements at 295 and 220 K[a,b]

radical/ tensor	isotropic value	principal values	eigenvector[e] ⟨*a*⟩	⟨*b*⟩	⟨*c*⟩
R2[c] $\mathbf{H}_\beta$	70.8(1)	76.1(2)	0.925(8)	0.248(22)	0.288(23)
		68.3(2)	0.150(170)	0.458(440)	−0.876(200)
		68.0(2)	0.349(83)	−0.853(230)	−0.386(450)
R2[d] $\mathbf{H}_\beta$	70.8(2)	76.4(3)	0.921(9)	0.264(24)	0.286(21)
		68.1(2)	0.273(320)	0.083(−)	−0.958(008)
		67.9(3)	0.276(312)	−0.961(95)	−0.005(−)
R2[d] $\mathbf{H}_\beta$1(N)	86.3(2)	95.8(3)	0.681(12)	−0.516(18)	−0.519(13)
		83.6(3)	0.182(44)	0.806(18)	−0.563(33)
		79.4(3)	0.709(15)	0.289(46)	0.643(33)
R2[d] $\mathbf{H}_\beta$2(N)	30.2(1)	40.9(3)	0.897(6)	0.270(13)	−0.349(12)
		25.5(2)	0.314(60)	0.163(179)	0.935(12)
		24.1(3)	0.310(60)	−0.949(30)	0.061(177)
R2[d] $\mathbf{H}_\beta$3(N)	10.2(1)	19.9(1)	0.199(14)	−0.032(14)	−0.980(03)
		5.4(3)	0.466(−)	−0.876(705)	0.123(234)
		5.3(3)	0.862(683)	0.481(−)	0.159(181)

[a] Hyperfine coupling tensor elements are given in units of MHz. [b] Uncertainties are given at the 95% confidence level in the last digit(s) of the quoted values. [c] From X-band ENDOR measurements at 295 K. [d] From K-band ENDOR measurements at 220 K. [e] Bond diretions:

crystallographic[26] C2−Cm bond direction	0.8000	0.5656	0.2007
recalculated C2−Cm bond direction	0.9317	0.2746	0.2376
recalculated C−H1(N) bond direction	0.7230	−0.4478	−0.5261
recalculated C−H2(N) bond direction	0.8190	0.3979	−0.4134
recalculated C−H3(N) bond direction	0.2787	0.1483	−0.9489

Figure 4c shows an X-band EIE spectrum associated with R2 ($B \| \langle a \rangle$). In Figure 4d a simulated absorption spectrum (X-band) is shown. This spectrum is calculated for $B \| \langle a \rangle$ from the four hyperfine coupling tensors (obtained from the K-band) for radical R2 given in Table 3. In addition, a nitrogen hyperfine interaction analogous to that of the corresponding radical in glycine[36] was used. (Principal values of the nitrogen hyperfine interaction were assumed to be 8.3, 8.2, and 5.5 MHz, scaled down from the glycine values[36] with the factor of the C_α spin densities, 0.75/0.90. The eigenvector for the minimum principal value was assumed to be along the perpendicular to the (N,Cm,C1) molecular fragment.) The small superhyperfine splitting pattern on the extreme outer features of the EPR spectrum in Figure 1b is in agreement with a nitrogen coupling of this order of magnitude. In Figure 6 are shown EIE spectra obtained from the K-band ENDOR spectra at 220 K. Clearly, the lower experimental spectrum in Figure 6 corresponds to the X-band EIE spectrum in Figure 4c. Also shown in Figure 6 are simulated absorption EPR spectra (K-band) at the orientations corresponding to the experimental EIE spectra. Figure 4e shows the EIE obtained from a partially deuterated alanine crystal at 295 K in a manner similar to that described for the spectrum in Figure 4c. An identical EIE spectrum was obtained in the 220 K K-band experiment. As expected for structure **2** if the amino protons are exchanged with deuterons, the 10-line pattern of Figure 4c and the ⟨*a*⟩-axis spectrum in Figure 6 are reduced to a four-line pattern upon deuteration. Figure 4f shows the simulated EIE spectrum of R2 along ⟨*a*⟩ (obtained as in Figure 4d) when the three amino proton couplings have been exchanged with the corresponding deuteron couplings. The agreement between the different EIE spectra and the simulated EPR spectra in nondeuterated as well as in deuterated crystals lends strong confidence to the assignment of radical R2 to structure **2**.

It is concluded that radical R2 is associated with a methyl proton interaction and with interactions with three exchangeable nonequivalent amino protons, structure **2**. The amino group is

not freely rotating (as, for example, in the corresponding radical in glycine[36]), but the amino protons are locked in positions close to those determined by neutron diffraction,[29] defined by the hydrogen-bonding interactions in the crystal. The lack of observable ENDOR from the amino protons at room temperature is ascribed to excessive thermal libration of the amino protons which significantly increases the ENDOR line width.

In the following, a few considerations of the geometrical configuration of radical R2 are made. First, it is assumed that upon hydrogen abstraction from C2, the carbon atom rehybridizes from sp^3 to sp^2. Since both the amino group and the carboxyl group are anchored by hydrogen bonding, it may be assumed that this rehybridization basically is associated with a movement of C2 into the plane of the atoms N, Cm, and C1. Recalculating the new C2−Cm bond direction yields the result presented in Table 3. This direction deviates 3.3° from the maximum principal value of the methyl coupling.

The Heller−McConnell relation[37] provides a relationship between the isotropic β-proton hyperfine interaction, the $2p^\pi$-spin density ρ^π at atom X, and structural parameters of a radical fragment >•X−Y−H:

$$a^\beta(\text{iso}) = \rho^\pi(B_0 + B_2 \cos^2 \theta)$$

B_0 and B_2 are constants and θ is the dihedral angle of the Y−H bond with respect to the plane of the X−Y bond and the LEO. Assuming a perfect sp^2 hybridization of the $-N^+H_3$ group, there are four unknowns in this relation, ρ^π, B_0, B_2, and θ, the dihedral angle for one of the protons (the two other angles are obtained as $\theta \pm 120°$). The isotropic values for the three amino proton couplings in Table 3 provide for three equations. The fourth equation may be obtained from the glycine results.[36] The dominant radical in single crystals of glycine exhibits a β-amino coupling of 54.7, 46.5, 46.0 MHz with the $2p^\pi$ spin density estimated from the α-proton coupling of this radical to be about 0.90 ($Q = -72$ MHz). For a freely rotating amino group, the Heller−McConnell relation becomes $a^\beta(\text{iso}) = \rho^\pi(B_0 + (1/2)B_2)$. For glycine, $a^\beta(\text{iso}) = 49.06$ MHz and with $\rho^\pi = 0.90$, the fourth equation $(B_0 + (1/2)B_2) = 54.51$ is obtained. Solving the four equations yields the following results for radical R2: $\rho^\pi = 0.77$, $B_0 = -4.3$ MHz, $B_2 = 117.6$ MHz, and $\theta = 7.3°$. The B values are similar to although somewhat larger than the corresponding values previously calculated.[38] With $\theta = 7.3°$ the two other dihedral angles are calculated to be 127.3° and −112.7°. Using the perpendicular to the fragment N, Cm, C1 as representative for the direction of the LEO, the crystallographic positions of the three amino protons in alanine correspond to dihedral angles of 3°, 118°, and −108° (note the deviation from trigonal symmetry), in good agreement with those calculated from the experimental data.

Figure 7 shows the results of simulation of the EPR spectra from nondeuterated crystals with the magnetic field along ⟨*c*⟩ and ⟨*a*⟩. The tensor data for radicals R1 and R2 in Tables 2 and 3 were used, together with a nitrogen hyperfine interaction for radical R2 as described above. The *g* values for R2 were measured from the EPR spectra and were found to be the same at both orientations ($g = 2.0034$). Line widths were measured from the experimental spectra. Finally, the relative weights (amounts of radicals) were estimated visually. The simulations very convincingly show that the model (structure **2**) and data arrived at can reproduce the composite experimental EPR spectra. For the simulated spectra shown in Figure 7 it was necessary to assume that 40% of the total radical population consisted of R2 radicals and 60% consisted of R1 (SAR). Simulations at other orientations yielded similar results. Simulations of single-crystal spectra do not necessarily yield the exact

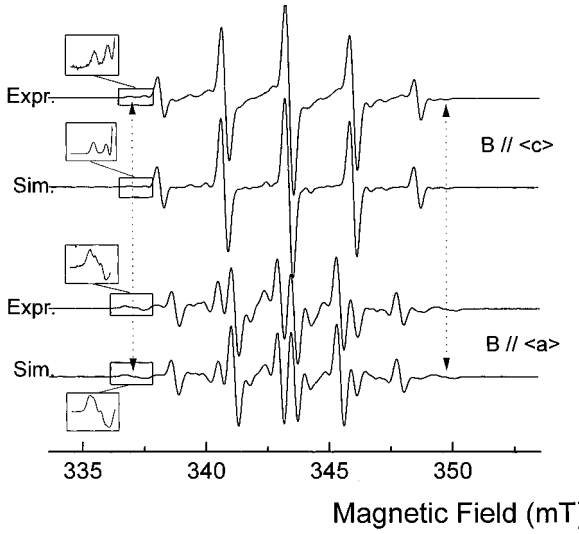

Figure 7. Experimental and simulated first-derivative X-band EPR spectra from an X-irradiated nondeuterated single crystal of L-α-alanine at 295 K with the external magnetic field parallel with ⟨*c*⟩ (top) and ⟨*a*⟩ (bottom). Parameters for the simulations are as described for Figures 3 and 4 and in the text. The relative amounts of radical R1 and radical R2 in the simulated spectra are 0.6:0.4. The dotted lines highlight the outer features due to radical R2.

TABLE 4: Magnetic Parameters for the Two Conformations of the R3 Radical in X-Irradiated Single Crystals of L-α-Alanine from ENDOR Measurements at 295 K[a,b]

radical/ tensor	isotropic value	principal values	eigenvector[c] ⟨*a*⟩	⟨*b*⟩	⟨*c*⟩
R3 H_β	39.5(1)	44.5(2)	0.954(08)	0.266(27)	0.141(29)
		37.3(2)	0.155(84)	−0.835(140)	0.528(270)
		36.8(2)	−0.258(56)	0.481(270)	0.837(172)
R3 $H_{\beta'}$	33.1(2)	37.7(2)	0.862(15)	0.428(27)	0.271(29)
		30.8(3)		⊥ above	
		30.8(3)		⊥ above	

[a] Hyperfine coupling tensor elements are given in units of MHz. [b] Uncertainties are given at the 95% confidence level in the last digit(s) of the quoted values. [c] Bond directions:

crystallographic[26] C−Cm bond direction	0.8000	0.5656	0.2007
recalculated C2−Cm bond direction	0.9317	0.2746	0.2376

relative amounts of the various resonance contributors; however, the general conclusion to be made is that in alanine samples X irradiated at room temperature, the two radicals R1 and R2 are present in comparable amounts. Extensive simulations of alanine powder spectra recorded at X-, K-, and Q-band microwave frequencies fully corroborate these conclusions (E. O. Hole and E. Sagstuen, results in preparation for publication).

3.3. Radical R3: A Minority Species. In Table 4, two hyperfine coupling tensors have been assigned to two conformations of radical R3. Both tensors are characteristic of a coupling between the unpaired electron and a (freely rotating) methyl group. The eigenvectors for the maximum principal values are both close to the crystallographic C2−Cm bond. The C2 spin densities of the two conformations are on the order of 35−45%, i.e., about half the magnitude of the methyl couplings associated with radicals R1 and R2 discussed above. Both couplings are associated with similar multiline EIE spectra. Since no other experimental evidence is yet available, an assignment of the radical structures necessarily must be tentative. However, one possibility is represented by structure **3** below. Depending upon the coplanarity (i.e. π-conjugation) of the $-NH_2$ group, the >C−H fragment and the carboxyl group, the unpaired spin density will be partially delocalized onto the

carbonyl oxygen as well as to the $-NH_2$ group, thus reducing the spin density at C2. Environmental factors, such as the actual site of amino deprotonation, may be important in directing the final radical geometry. Semiempirical molecular orbital calculations to be described in detail elsewhere[44] indicate that for Structure 3 (in an energy optimized geometry), about 20% of the spin resides at the nitrogen atom, about 45% at the central carbon atom C2, and, finally, about 25% at the carbonyl oxygen atom.

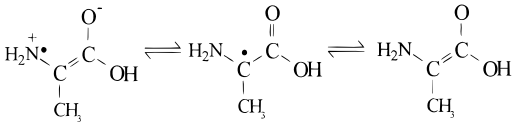

Structure 3

The same radical structure was previously suggested to become stabilized in X irradiated acidic and basic glasses of alanine.[20,21] Heck[21] used ^{15}N labeling to show that there is a significant contribution of nitrogen coupling to the resonance from this radical. He assumed the methyl coupling to be somewhat smaller (about 0.75 mT) than that given in Table 3. Sevilla,[20] however, suggested that the methyl coupling is 1.3 mT for the same species. The differences in the magnitude of the methyl coupling may be ascribed to effects of different matrixes. Recently, a similar radical was observed in glycine single crystals irradiated and measured at 295 K.[44]

3.4. ENDOR, EIE, and Spin Relaxation. Figure 8 shows ENDOR spectra obtained by monitoring the X-band EPR (given in the inset) at various field positions. The spectra are recorded at room temperature; thus the ENDOR lines associated with the amino protons in radical R2 are not observed. It is evident that the ENDOR response depends upon the values of the electron and nuclear spin quantum numbers of the various transitions. The ENDOR spectra labeled 1 and 5 are obtained from respectively the extreme low-field and the extreme high-field EPR lines of radical R2. Assuming positive hyperfine coupling constants for these β-protons, the extreme low-field position corresponds to $M_I = 3/2$ for both the methyl and amino proton nuclear quantum numbers. At this field position only the $M_s = 1/2$ ENDOR resonance is observed (labeled 1). Similarly, only the $M_s = -1/2$ transition resonance is observed (labeled 5) when the field is locked to the high-field EPR (corresponding to $M_I = -3/2$) from radical R2. A similar behavior is observed for radical R1 (ENDOR spectra labeled 2 and 4), but due to overlapping resonances, the ENDOR from both radicals R1 and R2 is obtained at these field positions. The center of the EPR contains overlapping resonance lines from each radical with both positive and negative nuclear quantum numbers; thus, when monitoring at the center field both branches of the ENDOR response are consequently observed.

It should be noted that in ENDOR spectrum 2 (monitoring $M_I = 3/2$ for the methyl of radical R1) the $M_s = +1/2$ branch of the α-proton coupling (high-frequency line) is observed together with the $M_s = +1/2$ branch of the methyl interaction (low-frequency branch). These lines are not observed in ENDOR spectrum 4 when monitoring $M_I = -3/2$. (The low-frequency ENDOR line of the a-proton coupling is at this orientation at about 5 MHz, it is always very weak, and it is not depicted in these spectra.) This behavior is characteristic of a spin system where the nuclear spin lattice relaxation rates (W_{1n}) are slow as compared to the electron spin−lattice relaxation rate (W_{1e}) and where, in addition, the electron spin−nuclear spin cross flip-flop relaxation rate W_{1x} (characterized by $\Delta M_s + \Delta M_I = 0$) is comparable to W_{1e}. Brustolon et al.[39]

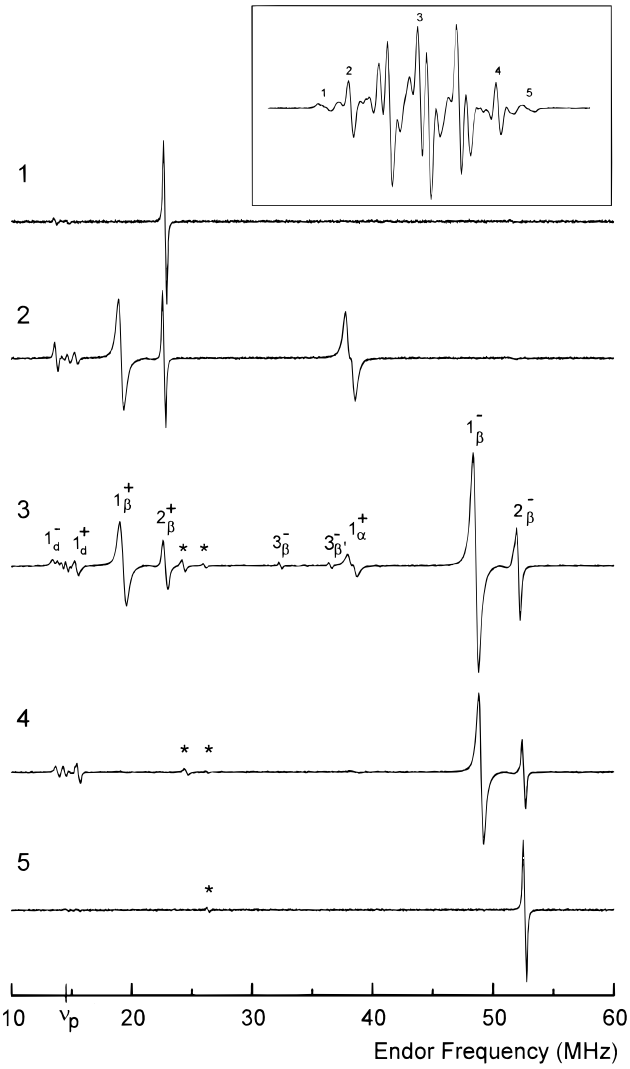

Figure 8. ENDOR spectra from a nondeuterated single crystal of L-α-alanine, X-irradiated at 295 K. The external magnetic field is parallel with ⟨*a*⟩. The inset shows the corresponding EPR spectrum. The various ENDOR spectra have been designated according to which position in the EPR the magnetic field was locked while recording the ENDOR. Resonance lines have been marked as described in the text (see also Figure 2). Lines marked with * are due to second harmonics of the two strongest ENDOR lines in the region about 50 MHz.

have previously observed a behavior similar to that depicted in Figure 8 for the SAR and related this to efficient W_{1x} relaxation induced by modulation of the isotropic (contact) methyl coupling due to methyl group rotation. These authors cleverly used these observations to deduce the dynamics of the methyl rotation and the electron spin−lattice relaxation rate.

As discussed by Kevan and Kispert[40] using a simple four-level spin system as an example, monitoring the $M_I = +1/2$ EPR line under these relaxation conditions will yield only the $M_s = +1/2$ ENDOR transition. Whether this is the low- or high-frequency line of the pair of possible ENDOR responses depends on the sign of the hyperfine coupling. Feher[41] used this to determine the sign of the nuclear *g* factor of ^{32}P. In the present case of alanine it is known the nuclear *g* factor for protons is positive. As easily recognized using, for example, an eight-level spin system as a simplified model, the observation of only the low-frequency line of one proton interaction together with only the high-frequency line of another proton interaction when monitoring an EPR line with a unique M_I quantum number sign combination shows that these two interactions exhibit different signs of their hyperfine coupling. Since this is as

expected for the α-proton and a β-proton interaction of radical R1 (SAR), the ENDOR labeled 2 in Figure 8 just yields further support to the interpretation of the radical structure of the SAR. Under the given relaxation circumstances this may be a method alternative to the so-called "double ENDOR" method[42] or pulse methods such as HYSCORE[43] to determine the relative signs of different hyperfine couplings in solids. As is clear from the above discussion, in the present case even the absolute signs are determined. In our laboratories we have recently observed similar behavior for the ENDOR response from the dominant radical in X-irradiated single crystals of glycine at room temperature.[44]

The asymmetry of the EIE spectra as shown in Figures 3 and 4 is just another consequence of the relaxation properties of the radical(s) described above. EIE is the enhancement of a saturated NMR transition upon sweeping the magnetic field and in turn partially saturating the different EPR transitions connected to this NMR transition. The incomplete EIE spectra obtained at 295 K are explained using the same considerations as above for why only one out of the pair of ENDOR lines associated with one coupling is observed, given an EPR transition. Similarly, the more complete EIE spectra observed at 220 K (Figure 6) are understood considering the reduced rate of methyl group rotation at this temperature and correspondingly decreased W_{1x} relaxation rate.

4. Discussion and Conclusions

The results in this paper leave no doubt that two radicals are stabilized in comparable amounts in L-alanine single crystals after X-irradiation at room temperature. One of these is the well-known deamination product, the SAR (given in structure **1**), whereas the second species is the H-abstraction radical, shown in structure **2**. This second radical yields a wide EPR with broad lines, contributing to the overall features of the alanine resonance. In addition a third radical species is present at room temperature. This apparently is a minority product contributing to the central part of the alanine spectrum only.

The alanine radical exhibiting structure **2** was previously observed in irradiated frozen H_2SO_4/Fe^{2+} and BeF_2 glasses of alanine, most probably formed by •H and •OH attack, respectively.[21] The hyperfine coupling parameters for this radical in the frozen glasses agree well with those given in Table 3.

It is interesting to note that the alanine decarboxylation product is not observed either in the present or in previous studies. Considering the radiation chemistry of amino acids,[22] it is generally accepted that the deamination product is formed from a (protonated) anion, whereas the cation decomposes by decarboxylation.[9,16] The results for alanine agree with this with regard to the reductive pathway. On the oxidation side, however, the situation is more unclear. Although some disagreement exists, previous EPR and ENDOR work on alanine seems to indicate that the pristine cation initially deprotonates at the amino position[45,46] and that the spin density is excessively delocalized over the entire molecular skeleton.[45−47] Furthermore, there is some evidence indicating that the deprotonated cation of alanine subsequently decarboxylates.[16,22] This is supported by a combined pulse radiolysis/EPR study[48] showing that the activation energy for decarboxylation of the glycine cation and decomposition of the alanine cation exhibit the same activation energy. In the aliphatic amino acids the decarboxylation product is very unstable.[22] One possible pathway for the further reaction of the decarboxylation product is intermolecular hydrogen transfer involving a neighboring molecule, forming an H-abstraction radical (centered at the central carbon atom C2) and a diamagnetic species.[16,22,49] Apparently, this pathway may be operative for alanine. At present, there are no detailed studies of the oxidative alanine radiation-induced processes supporting this hypothesis. In glycine, the major radical products immediately after irradiation at room temperature are the products $H_3N^+-{}^\bullet CH-COO^-$ (**I**) and $^\bullet CH_2COOH$ (**II**).[22,44] Product **II** is due to deamination of the pristine glycine anion. The mechanism leading to product **I**, which is similar to radical R2 in alanine, is still controversial, but net decarboxylation of the pristine oxidation product followed by intermolecular hydrogen abstraction has been suggested as one plausible process.[22]

There have been several studies by spin trapping of alanine radicals initially formed in polycrystalline samples irradiated at room temperature.[50] In none of the published studies has radical R2 of the present work been detected, only radical R1 (SAR). This highlights the cautionary statements of Riesz and co-workers[50] on the limitation of the spin-trapping method with regard to ability and efficiency of trapping secondary radicals.

For the last decade alanine has gained wide application for dosimetry purposes. It has been assumed that for alanine the solid-state radical population consists of only one radical, the SAR. Thus, all spectral variations with regard to line amplitudes and integrated spectra with radiation dose and microwave power have been assigned to various properties of this radical.[17−19] Now, however, with the realization that the alanine spectrum consists of two components in similar relative amounts, in addition to a weaker third component, some reevaluation of previous results should be made. All three radicals exhibit line components in the center of the polycrystalline EPR spectra and thus contribute to the peak-to-peak amplitude used to monitor the radiation dose. In particular, the two major spectral components may have different microwave power saturation properties as well as dose saturation properties, and they may exhibit differences in other properties as well, such as fading characteristics and radiation quality response. Efforts to elucidate the properties of radical R2, in combination with improved calibration data and eventual spectral subtraction techniques, may improve the usability of alanine as a radiation dosimeter in the lower dose range. Efforts toward this goal are presently being made in our laboratories.

Acknowledgment. This work was supported in part by a grant from the Norwegian Research Foundation. Discussions with Professor Anders Lund are appreciated.

References and Notes

(1) Morton, J. R.; Horsfield, A. *J. Chem. Phys.* **1961**, *35*, 1142. Horsfield, A.; Morton, J. R.; Whiffen, D. H. *Mol. Phys.* **1962**, *4*, 425. Horsfield, A.; Morton, J. R.; Whiffen, D. H. *Mol. Phys.* **1962**, *5*, 115.
(2) Miyagawa, I.; Gordy, W. *J. Chem. Phys.* **1960** *32*, 255.
(3) Miyagawa, I.; Itoh, K. *J. Chem. Phys.* **1962**, *36*, 2157.
(4) Sinclair, J. W.; Hanna, M. W. *J. Phys. Chem.* **1967**, *71*, 84. Sinclair, J. W.; Hanna, M. H. *J. Chem. Phys.* **1969**, *50*, 2125.
(5) Minegishi, A.; Shinozaki, Y.; Meshitsuka, G. *J. Chem. Soc. Jpn.* **1967**, *40*, 1549. Minegishi, A.; Shinozaki, Y.; Meshitsuka, G. *J. Chem. Soc. Jpn.* **1968**, *41*, 3035.
(6) Miyagawa, I.; Tamura, N.; Cook, J. W. *J. Chem. Phys.* **1969**, *51*, 3520.
(7) Davidson, R.; Miyagawa, I. *J. Chem. Phys.* **1970**, *52*, 1727.
(8) Friday, E. A.; Miyagawa, I. *J. Chem. Phys.* **1971**, *55*, 3589.
(9) Muto, H.; Iwasaki, I. *J. Chem. Phys.* **1973**, *59*, 4821.
(10) Muto, H.; Iwasaki, I.; Ohkuma, J. *J. Magn. Reson.* **1977**, *25*, 327.
(11) Kuroda, S.-i.; Miyagawa, I. *J. Chem. Phys.* **1982**, *76*, 3933.
(12) Matsuki, K.; Miyagawa, I. *J. Chem. Phys.* **1982**, *76*, 3945.
(13) Brustolon, M.; Segre. U. *Appl. Magn. Reson.* **1994**, *7*, 405.
(14) Nam, J. W.; Regulla, D. F. *Appl. Radiat. Isot.* **1989**, *40*, 953.
(15) Bradshaw, W. W.; Cadena, D. G.; Crawford, G. W.; Spetzler, H. A. W. *Radiat. Res.* **1962**, *17*, 11.
(16) Iwasaki, M. *MTP International Review of Science; Physical Chemistry Series One, Vol. 4;* Butterworth University Park Press: New York, 1972; p 317.

(17) Simmons, J. A. *J. Chem. Phys.* **1962**, *36*, 469.
(18) Arber, J. M.; Sharpe, P. H. G.; Joly, H. A.; Morton, J. R.; Preston, K. F. *Appl. Radiat. Isotop.* **1991**, *42*, 665.
(19) Ciesielski, B.; Wielopolski, L. *Radiat. Res.* **1994**, *140*, 105.
(20) Sevilla, M. D. *J. Phys. Chem*. **1970**, *74*, 2096. Sevilla, M. D.; Brooks, V. L. *J. Phys. Chem.* **1973**, *77*, 2954.
(21) Heck, T. Dissertation, University of Saar, Saarbrücken, Germany, 1993.
(22) Box, H. C. *Radiation Effects, ESR and ENDOR Analysis*; Academic Press: New York, 1977.
(23) Sinclair, J. *J. Chem. Phys.* **1971**, *55*, 245.
(24) Sagstuen, E.; Hole, E. O.; Haugedal, S. R.; Lund, A.; Eid, O. I.; Erickson, R. *Nukleonika* **1997,** *42*, 353.
(25) Trammell, G. T.; Zeldes, H.; Livingston, R. *Phys. Rev*. **1958**, *110*, 630
(26) McConnell, H. M.; Heller, C.; Cole, T.; Fessenden, R. W. *J. Am. Chem. Soc.* **1960**, *82*, 766.
(27) Simpson, H. J.; Marsh, R. E. *Acta Crystallogr*. **1966**, *20*, 550.
(28) Dunitz, J. D.; Ryan, R. R. *Acta Crystallogr*. **1966**, *21*, 617.
(29) Lehmann, M. S.; Koetzle, T. F.; Hamilton, W. C. *J. Am. Chem. Soc*. **1972**, *94*, 2657.
(30) Schonland, D. *Proc. Phys. Soc. (London)* **1958**, *73*, 788.
(31) (a) Andersen, M.; Sagstuen, E.; Henriksen, T.; Lindgren, M. *J. Magn. Reson.* **1987**, *71*, 461. (b) Nelson, W. H.; Hole, E. O.; Sagstuen, E.; Close, D. M. *Int. J. Radiat. Biol.* **1988**, *54*, *963.*
(32) Nelson, W. H. *J. Magn. Reson.* **1980**, *38*, 71.
(33) McConnell, H. M.; Robertson, R. E. *J. Phys. Chem.* **1957**, *61*, 1018.
(34) Bernhard, W. A. *Adv. Radiat. Biol.* **1981**, *9*, 199.
(35) Bernhard, W. A. *J. Chem. Phys.* **1984**, *81*, 5928
(36) Morton, J. R. *J. Am. Chem. Soc.* **1964**, *86*, 2325. Collins, M. A.; Whiffen, D. H. *Mol. Phys.* **1966**, *10*, 317. Hedberg, A.; Ehrenberg, A. *J. Chem. Phys.* **1968**, *48*, 4822. Deigen, M. F.; Krivenko, V. G.; Pulatova, M. K.; Ruban, M. A.; Teslenko, V. V.; Kayushin, L. P. *Biofizika* **1973**, *18*, 235.
(37) Heller, C.; McConnell, H. M. *J. Chem. Phys.* **1960**, *32*, 1535.
(38) Gordy, W. *Theory and Applications of Electron Spin Resonance*; John Wiley & Sons: New York, 1980; p 237.
(39) Brustolon, M.; Cassol, T.; Micheletti, L.; Segre, U. *Mol. Phys.* **1986**, *57*, 1005. Brustolon, M. *Radiat. Phys. Chem.* **1995,** *45*, 953.
(40) Kevan, L.; Kispert, L. D. *Electron Spin Double Resonance Spectroscopy*; John Wiley & Sons: New York, 1976.
(41) Feher. G.; Fuller, C. S.; Gere, E. A. *Phys. Rev.* **1957**, *107*, 1462.
(42) Cook, R. J.; Whiffen, D. H. *Proc. Phys. Soc.* **1964**, *84*, 845. Hampton, D. A.; Alexander, C., Jr. *J. Chem. Phys.* **1973**, *58*, 4891.
(43) Höfer, P.; Grupp, A,; Nebenführ, H.; Mehring, M. *Chem. Phys. Lett.* **1986**, *132*, 279.
(44) Sanderud, A.; Sagstuen, E. Manuscript in preparation.
(45) Muto, H.; Iwasaki, M.; Takahashi, Y. *J. Chem. Phys.* **1977**, *66*, 1943.
(46) Minegishi, A. *J. Phys. Chem.* **1977**, *81*, 1688.
(47) Friday, E. A.; Miyagawa, I. *J. Chem. Phys.* **1971**, *55*, 3589.
(48) Lund, A.; Nilsson, G.; Samskog, P.-O. *Radiat. Phys. Chem.* **1986**, *27*, 111.
(49) Sinclair, J. *J. Chem. Phys.* **1971**, *55*, 245. Horan, P. K.; Henriksen, T.; Snipes, W. *J. Chem. Phys.* **1970**, *52*, 432.
(50) Minegishi, A.; Bergene, R.; Riesz, P. *Int. J. Radiat. Biol.* **1980**, *38*, 627. Lion, Y.; Denis, G.; Mossoba, M. M.; Riesz, P. *Int. J. Radiat. Biol.* **1983**, *43*, 71.